Study of the confining of Ca^+ ions in a Penning trap

Sigurd S. Vargdal, Brage A. Trefjord, Nils E. C. Taugbøl and Frida O. Sørensen*
University of Oslo, Department of Physics
(Dated: January 13, 2023)

We want to study the Penning trap, which is a device designed to confine charged particles using an electric and a magnetic field. Lacking such a device, we analyze its functionality through analytical and numerical investigation. We model the Penning trap by simulating the movement of Ca^+ ions inside, using two numerical methods: forward Euler and 4^{th} order Runge-Kutta. We also calculated the particles' trajectories in the trap analytically for one particle for comparison with our numerical methods. We ran different simulations for different amounts of particles in the Penning trap, with and without Coulomb interactions, and with both static and time-dependent electric potentials. The trajectory of the particles from using the 4^{th} order Runge-Kutta method correspond well with our analytical expression, while the forward Euler method deviates more. We also get an error convergence rate of 1.46 for forward Euler, and an error convergence rate of 1.27 for the Runge-Kutta method. From this we see that the error of forward Euler converges faster than the error of Runge-Kutta, even though the error of Runge-Kutta is smaller. We also explore resonance frequencies for a time-dependent applied electric field and find that resonance pushes the particles out at multiples of the axial angular frequency $\omega_z \approx 0.6936$ MHz.

Keywords: Penning trap, forward Euler, 4^{th}-order Runge-Kutta

I. INTRODUCTION

To find and measure fundamental particle properties requires the ability to confine particles in a controlled environment. In the early 20^{th} century, F. M. Penning (1894-1953) found a way of extending the time electrons spent in a vacuum gauge by adding a magnetic field which would put them in a radial path along the magnetic field lines [1]. This eventually led to H. G. Dehmelt (1922-2017) building the first device that, with both electric and magnetic fields, could confine (store) electrons. A device which he named Penning trap and which earned him a shared Nobel Prize in 1989 [2].

In this report we seek to understand how a Penning trap constraints the path of positively charged particles in such a way that they become confined within the device. In our case we will be studying Ca^+ ions. As we are not in possession of such a device, we will simulate the path of the particle(s) using either analytical or numerical methods. Confining a single charged particle in a Penning trap is demanding though possible [3]. This leads us to explore how effective a Penning trap can be at confining greater numbers of similar particles which interact with one another. A numerical approach will be needed in order to simulate such a confinement.

The report is structured as follows. First, we introduce the theory behind the Penning trap. We derive relevant analytical expressions for our understanding of the ion confinement device. Second, we introduce numerical methods for the simulation of the path of the particles in the device, namely forward Euler and 4^{th}-order Runge-Kutta. We compare these two methods against a numerical solution. Finally we present and discuss our results. For different trial simulations using one to two ions and more general simulation with a greater number of ions to find the efficiency of the Penning trap.

II. METHOD

A. Penning trap

A charged atomic particle's path is affected by external magnetic, electric and gravitational fields. We will neglect the gravitational field given the low mass of the particle. The magnetic and electric fields act upon the particle by exercising a force known as the Lorentz force which is given by

$$\boldsymbol{F} = q\boldsymbol{E} + q\boldsymbol{v} \times \boldsymbol{B} \tag{1}$$

where $\boldsymbol{E}$ is the electric field, q is is the charge of the particle, $\boldsymbol{v}$ is the velocity of the particle and $\boldsymbol{B}$ is the magnetic field. This force affects the particle's path in time through Newton's second law of motion which, though it is well known, is given here:

$$\sum_i \boldsymbol{F}_i = m\ddot{\boldsymbol{r}} \tag{2}$$

where m is the mass of the particle (or object in question) and $\ddot{\boldsymbol{r}}$ is the second derivative of the position $\boldsymbol{r}$ with respect to time.

* Repository: https://github.com/NilsECT/FYS3150/tree/main/Project_3/

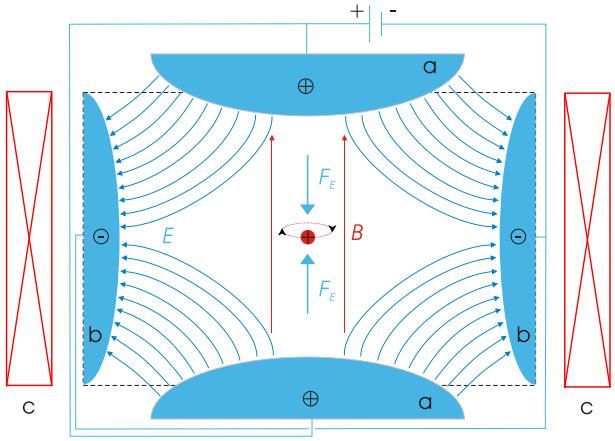

Figure 1: Simple illustration of the Penning trap. The blue arrows represent the electric field going from electrodes a to b. The magnets, c, create the magnetic field represented by the red arrows. The red dot in the center represents a positively charged particle. The red circle with arrows show the path of the particle in which it is forced. Illustration by Arian Kriesch Akriesch [4]

We study an ideal Penning trap where the electric field created within the trap is defined by the electric potential applied to the electrodes of the trap through

$$\boldsymbol{E} = -\nabla V \tag{3}$$

where V is the electric potential which, in our case, is given by

$$V(x, y, z) = \frac{V_0}{2d^2}(2z^2 - x^2 - y^2) \tag{4}$$

where V_0 is the potential applied, d is the characteristic dimension of the system and x, y and z are the position coordinates of the particle. This characteristic dimension represents the length scale between the two electrodes in figure 1.

We can see from figure 1 that the electric field will trap a positively charged particle in the z direction. In turn the magnets will trap said particle in the center of the trap in the xy-plane by applying a magnetic field

$$\boldsymbol{B} = (0, 0, B_0) \tag{5}$$

where $B_0 > 0$ is the magnetic field strength.

The applied potential V_0 can also be time-dependent, which is the case for an oscillating applied potential. For example, the potential can be expressed as

$$V_0 \to V_0(1 + f\cos(\omega_V t)) \tag{6}$$

where V_0 is the initial applied potential (from equation (4)), f is the amplitude, and ω_V is the angular frequency of the applied potential.

From equations (1) and (2) we can derive a set of differential equations that describe a charged particle's movement within the Penning trap:

$$\ddot{z} + \omega_z^2 z = 0 \tag{7}$$

$$\ddot{x} - \frac{1}{2}\omega_z^2 x(t) - \omega_0 \dot{y} = 0 \tag{8}$$

$$\ddot{y} - \frac{1}{2}\omega_z^2 y(t) + \omega_0 \dot{x} = 0 \tag{9}$$

where $\omega_z = \sqrt{\frac{2qV_0}{md^2}}$ and $\omega_0 = \frac{qB_0}{m}$. The full derivation can be found in Appendix A. We note that $x(t)$ and $y(t)$ can be written as x and y respectively.

Equations (8) and (9) are coupled. The two equations can be combined by extending the mathematics into the complex plane, such that $f(t) = x(t) + iy(t)$ is a complex function whose real part is the x-position and whose imaginary part is the y-position. Differentiating $f(t)$ twice with respect to time gives

$$\ddot{f} = \omega_0(\dot{y} - i\dot{x}) + \frac{1}{2}\omega_z^2(x + iy). \tag{10}$$

Using $i\dot{f} = i\dot{x} - \dot{y}$, we obtain a single complex differential equation

$$\ddot{f} + i\omega_0 \dot{f} - \frac{1}{2}\omega_z^2 f = 0. \tag{11}$$

The general solution for equation 11 is

$$f(t) = A_+ e^{-i(\omega_+ t + \phi_+)} + A_- e^{-i(\omega_- t + \phi_-)}. \tag{12}$$

where ϕ_+, ϕ_- are constant phases, and the amplitudes A_+, A_- are positive.

In the case of the Penning trap we require a bounded solution for the motion in the xy-plane. That is $|f(t)| < \infty$ as $t \to \infty$. From equation 12, we see that the absolute value of $f(t)$ diverges if $\omega_\pm$ is a multiple of i. Therefore, we must ensure that $\omega_\pm$ is real for any ω_0, ω_z. This constraint means that

$$Im[\omega_\pm] = Im\left[\frac{\omega_0 \pm \sqrt{\omega_0^2 - 2\omega_z^2}}{2}\right] = 0. \tag{13}$$

Which implies that

$$\omega_0^2 > 2\omega_z^2 \tag{14}$$

since we know that $\omega_0 = \frac{qB_0}{m}$ is a real number.

This allows us to relate the Penning trap parameters (B_0, V_0, d) to the properties of the particle (q, m) such that

$$\frac{q}{m} > \frac{4V_0}{B_0 d^2}. \tag{15}$$

is the condition for the particle to be bounded in the xy-plane.

Let R_+ and R_- be the upper and lower bounds, respectively, on the distance between the particle and the origin in the xy-plane. The absolute value $|f(t)|$ can be written as

$$|f(t)| = \sqrt{A_+^2 + A_-^2 + 2A_+A_- \cos\Big[-(\omega_+ t + \phi_+) + (\omega_- t + \phi_-)\Big]}. \tag{16}$$

This equation (16) attains its maximum when both of the exponents in (12) are equal to zero. In that case, the exponential terms will be $e^0 = 1$, meaning that

$$f(t) = R_+ = A_+ + A_-. \tag{17}$$

Equation (12) is a solution for a single charged particle in a Penning trap. In the case of trying to catch multiple charged particles in a Penning trap, equations (8), (9) and (7) must include the Coulomb force from all other charged particles. These equations then become:

$$\ddot{z}_i + \omega_{z,i}^2 z_i - k_e \frac{q_i}{m_i} \sum_{j \neq i} q_j \frac{z_i - z_j}{|\boldsymbol{r}_i - \boldsymbol{r}_j|^3} = 0 \tag{18}$$

$$\ddot{x}_i - \frac{1}{2}\omega_{z,i}^2 x_i(t) - \omega_0 \dot{y}_i - k_e \frac{q_i}{m_i} \sum_{j \neq i} q_j \frac{x_i - x_j}{|\boldsymbol{r}_i - \boldsymbol{r}_j|^3} = 0 \tag{19}$$

$$\ddot{y}_i - \frac{1}{2}\omega_{z,i}^2 y_i(t) + \omega_0 \dot{x}_i - k_e \frac{q_i}{m_i} \sum_{j \neq i} q_j \frac{y_i - y_j}{|\boldsymbol{r}_i - \boldsymbol{r}_j|^3} = 0 \tag{20}$$

where k_e is the Coulomb constant and, i and j are the particle indices. We note that the Coulomb forces make these differential equations non-linear and as such we will not attempt to solve them analytically.

B. Algorithms

The non-linearity of the differential equations we need to solve invite us to use numerical methods. We remind the reader that numerical methods are an *approximation*, which implies that they carry with them a certain uncertainty based on their local and global errors.

Instead of trying to solve a set of coupled non-linear second-order differential equations, for a number $N > 1$ of particles, we will simplify the differential equations to be of first order. Given a set of initial conditions we will calculate the forces acting on each particle. If we express $\ddot{\boldsymbol{r}}$ as $\dot{\boldsymbol{v}}$, we have from equation 2

$$\dot{\boldsymbol{v}} = \frac{\sum_i \boldsymbol{F}_i}{m} \tag{21}$$

and then we have

$$\dot{\boldsymbol{r}} = \boldsymbol{v}. \tag{22}$$

We now have a set of coupled first-order differential equations. To solve this set of differential equations for a chosen number N of particles we will employ the forward Euler and 4$^{\text{th}}$-order Runge-Kutta algorithms to simulate the particles' path through a Penning trap.

Algorithm 1 Forward Euler for coupled differential equations

```
v_0 ← [v_x, v_y, v_z]      ▷ Set initial conditions for velocity
r_0 ← [r_x, r_y, r_z]      ▷ Set initial conditions for position
h ← T/n                    ▷ Compute the stepsize
for i = 1, 2, ..., n do
    a = F/m                ▷ Compute acceleration
    v_i ← v_{i-1} + ah     ▷ Calculate next v step
    r_i ← r_{i-1} + v_{i-1}h   ▷ Calculate next r step
```

1. *Forward Euler*

For forward Euler we discretize equation 21 by approximating the first-order derivative using a time step h in order to find an expression for $\boldsymbol{v}$ at a following timestep:

$$\dot{\boldsymbol{v}} = \frac{\boldsymbol{F}}{m} \tag{23}$$

$$\frac{\boldsymbol{v}_{i+1} - \boldsymbol{v}_i}{h} + \mathcal{O}(h) = \frac{\sum_i \boldsymbol{F}_i}{m} \tag{24}$$

$$\boldsymbol{v}_{i+1} = \boldsymbol{v}_i + h\frac{\sum_i \boldsymbol{F}_i}{m} + \mathcal{O}(h^2). \tag{25}$$

Where we've simplified $\sum_i \boldsymbol{F}_i$ to $\boldsymbol{F}$ and the timesteps are denoted by the indices i. Truncating at $\mathcal{O}(h^2)$ gives us a local error of order $\mathcal{O}(h^2)$ for the approximated value of $\boldsymbol{v}$ at timestep $i+1$. Following the same procedure for $\boldsymbol{r}$ as for $\boldsymbol{v}$ we have algorithm 1. Doing forward Euler n times, when $n \propto 1/h$ gives us a global error proportional to $\mathcal{O}(nh^2) = \mathcal{O}(h)$. Each timestep of algorithm 1 must be computed for every particle at the same time as their positions affect the forces acting on each other. We note that forward Euler is a single-step first-order algorithm. That is it requires only one step to compute the next and its global error scales with $\mathcal{O}(h)$.

2. *4^{th} order Runge-Kutta*

Another method that can be used to solve the discretized set of coupled differential equations, is the 4$^{\text{th}}$ order Runge-Kutta method. Instead of using $\frac{\boldsymbol{F}}{m}$ and $\boldsymbol{v}_{i+1}$ as slopes for $\boldsymbol{v_i}$ and $\boldsymbol{r}_i$ (respectively), 4$^{\text{th}}$ order Runge-Kutta uses four different estimates for the slopes of each equation. The slopes are estimated by com-

puting $k_{i,r}$ and $k_{i,v}$, $i \in 1,2,3,4$, which give us the corresponding changes in the position and velocity.

The first shifts $k_{1,r}$ and $k_{1,v}$ are computed simply by using the same slopes as in the forward Euler method, meaning $k_{1,r} = h\boldsymbol{v}_i$ and $k_{1,v} = h\frac{\boldsymbol{F}}{m}$.

For some systems, the sum of the forces acting on the particle $\boldsymbol{F}$ may depend on the position or velocity of the particle. This is for example the case for the Coulomb force, whose strength (and direction) depends on the position of the particle relative to the other particles in the system. Therefore, we need to update the positions and velocities of every particle (using $k_{1,r}$ and $k_{1,v}$), before we continue to improve our estimation for the slopes. We update $\boldsymbol{r}$ and $\boldsymbol{v}$ using $k_{1,r}$ and $\boldsymbol{v}_i$, and advancing to the midpoint $t_i + \frac{h}{2}$ with the forward Euler method. This means that for a single particle, we compute:

$$\boldsymbol{v}_{i+1/2} = \boldsymbol{v}_i + k_{1,v}/2 = \boldsymbol{v}_i + \frac{h}{2}\frac{\boldsymbol{F}_i}{m} \tag{26}$$

$$\boldsymbol{r}_{i+1/2} = \boldsymbol{r}_i + k_{1,r}/2 = \boldsymbol{r}_i + \frac{h}{2}\boldsymbol{v}_i \tag{27}$$

where $\boldsymbol{F}_i$ denotes the sum of forces at t_i and h is the stepsize.

Further, we improve our estimations for $\boldsymbol{r}_{i+1/2}$ and $\boldsymbol{v}_{i+1/2}$ by using the slopes at the midpoint. This means that the slopes of position and velocity are $\boldsymbol{v}_{i+1/2}$ and $\frac{\boldsymbol{F}_{i+1/2}}{m}$ respectively, where $\boldsymbol{F}_{i+1/2}$ denotes the sum of the forces acting upon the particle at the midpoint. These slopes are used to compute $k_{2,r}, k_{2,v}$. Then we advance from t_i to $t_{i+1/2}$ again, using the improved slopes:

$$\boldsymbol{v}_{i+1/2} = \boldsymbol{v}_i + k_{2,v}/2 = \boldsymbol{v}_i + \frac{h}{2}\frac{\boldsymbol{F}_{i+1/2}}{m} \tag{28}$$

$$\boldsymbol{r}_{i+1/2} = \boldsymbol{r}_i + k_{2,r}/2 = \boldsymbol{r}_i + \frac{h}{2}\boldsymbol{v}_{i+1/2} \tag{29}$$

For the third pair of k-values, we use the slopes $\boldsymbol{v}_{i+1/2}$ and $\frac{\boldsymbol{F}_{i+1/2}}{m}$ from the improved advancement above. Using these slopes, we advance to the next timestep t_{i+1}. This yields

$$\boldsymbol{v}_{i+1} = \boldsymbol{v}_i + k_{3,v} = \boldsymbol{v}_i + h\frac{\boldsymbol{F}_{i+1/2}}{m} \tag{30}$$

$$\boldsymbol{r}_{i+1} = \boldsymbol{r}_i + k_{2,r} = \boldsymbol{r}_i + h\boldsymbol{v}_{i+1/2} \tag{31}$$

Lastly, we compute the shifts

$$k_{4,r} = h\boldsymbol{v}_{i+1} \tag{32}$$

$$k_{4,v} = h\frac{\boldsymbol{F}_{i+1}}{m} \tag{33}$$

using the updated velocity $\boldsymbol{v}_{i+1}$ and force $\boldsymbol{F}_{i+1}$ at position $\boldsymbol{r}_{i+1}$. The final succeeding steps $\boldsymbol{r}_{i+1}, \boldsymbol{v}_{i+1}$ are computed using a weighted sum of the k_i's:

$$\boldsymbol{v}_{i+1} = \boldsymbol{v}_i + \frac{1}{6}\Big(k_{1,v} + 2k_{2,v} + 2k_{3,v} + k_{4,v}\Big) \tag{34}$$

$$\boldsymbol{r}_{i+1} = \boldsymbol{r}_i + \frac{1}{6}\Big(k_{1,r} + 2k_{2,r} + 2k_{3,r} + k_{4,r}\Big) \tag{35}$$

Since we compute the change in $\boldsymbol{r}, \boldsymbol{v}$ in four steps, the 4^{th} order Runge-Kutta is a fourth order method, meaning the global error scales as $\mathcal{O}(h^4)$ and the local error scales as $\mathcal{O}(h^5)$.

The full algorithm for the 4^{th} order Runge-Kutta method can be seen in algorithm 2. The method is a single-step method, as the discretized solutions are advanced from t_i to t_{i+1} in a single step. Even though the method contains several intermediate steps to the midpoint, the final advancement is performed in one step.

Algorithm 2 4^{th} order Runge-Kutta for coupled differential equations

$v_0 \leftarrow [v_x, v_y, v_z]$ ▷ Set initial conditions for velocity
$r_0 \leftarrow [r_x, r_y, r_z]$ ▷ Set initial conditions for position
$h \leftarrow T/n$ ▷ Compute the stepsize
for $i = 1, 2, \ldots, n$ **do**
  $k_{1,r} = hv_i$ ▷ Compute shifts
  $k_{1,v} = h\frac{\boldsymbol{F}_i}{m}$
  $r_{i+1/2} \leftarrow r_i + k_{1,r}/2$ ▷ Advance to midpoint
  $v_{i+1/2} \leftarrow v_i + k_{1,v}/2$
  $k_{2,r} = hv_{i+1/2}$ ▷ Compute shifts at midpoint
  $k_{2,v} = h\frac{\boldsymbol{F}_{i+1/2}}{m}$
  $r_{i+1/2} \leftarrow r_i + k_{2,r}/2$ ▷ Advance to midpoint again
  $v_{i+1/2} \leftarrow v_i + k_{2,v}/2$
  $k_{3,r} = hv_i$ ▷ Compute shifts at midpoint again
  $k_{3,v} = h\frac{\boldsymbol{F}_{i+1/2}}{m}$
  $r_{i+1} \leftarrow r_i + k_{3,r}$ ▷ Advance to next step
  $v_{i+1} \leftarrow v_i + k_{3,v}$
  $k_{4,r} = hv_{i+1}$ ▷ Compute shifts
  $k_{4,v} = h\frac{\boldsymbol{F}_{i+1}}{m}$
  ▷ Update state with weighted shifts
  $r_{i+1} \leftarrow r_i + \frac{1}{6}(k_{1,r} + 2k_{2,r} + 2k_{3,r} + k_{4,r})$
  $v_{i+1} \leftarrow v_i + \frac{1}{6}(k_{1,v} + 2k_{2,v} + 2k_{3,v} + k_{4,v})$

III. RESULTS AND DISCUSSION

We first compare the relative error that the numerical methods yields to the analytical solution we have for a single particle in the Penning trap. The initial position and velocity, charge and mass for this particle can be found in table I in the row labeled "Particle 1". The Penning trap we simulated had a magnetic field strength $B_0 = 9.65 \cdot 10^1 \frac{u}{(\mu s)e}$, an applied electric

Values	$\vec{r}$ [μm]	$\vec{v}$ [μm/μs]	q [e]	m [u]
Particle 1	$(20, 0, 20)$	$(0, 25, 0)$	1	40.078
Particle 2	$(25, 25, 0)$	$(0, 40, 5)$	1	40.078

Table I: Table of initial position $\vec{r}$, initial velocity $\vec{v}$, charge q and mass m for the two simulated particles in the first part of our simulations. Here e is the elementary charge, and u is the atomic mass unit.

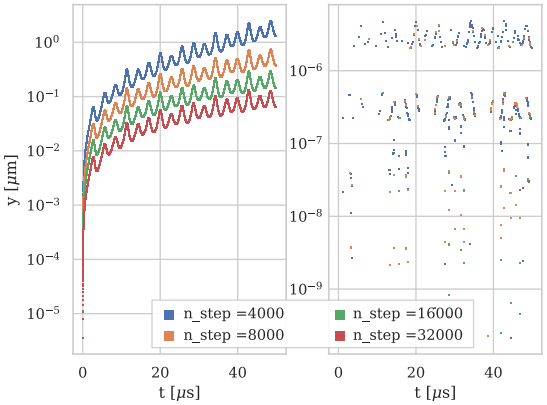

Figure 2: Relative error of the forward Euler (left) and 4^{th}-order Runge-Kutta methods for simulations of different stepsizes. Notice the that the relative error of th forward Euler method is several orders of magnitude greater than that of the 4^{th}-order Runge-Kutta method.

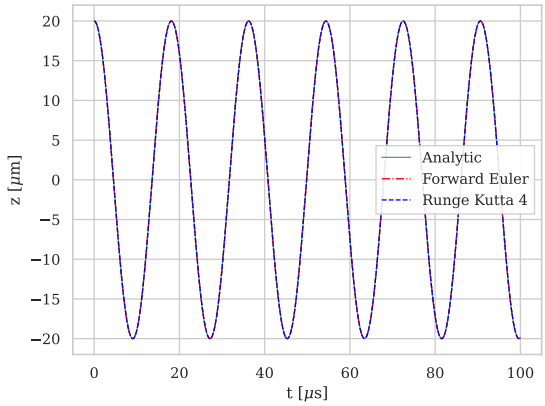

(a) Trajectory in the z direction.

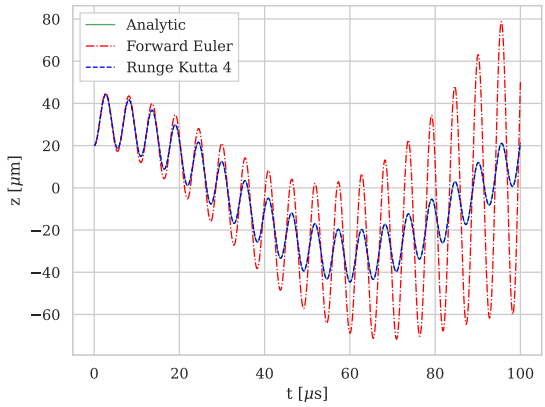

(b) Trajectory in the x direction.

Figure 3: Trajectories for a single particle in the Penning trap. The initial conditions for this particle can be found in table I, in the row labeled "Particle 1". This shows the analytical solution along with the path computed by the forward Euler and 4^{th}-order Runge-Kutta methods for a duration of 100μs and N= 4000 time steps.

potential $V_0 = 2.41 \cdot 10^6 \frac{\text{u}(\mu\text{m})^2}{(\mu\text{s})^2 e}$, and a characteristic dimension $d = 500\mu$m. Here u is the atomic mass unit, and e is the elementary charge. The relative error as a function of time with varying h (stepsizes) is shown in Figure 2. From this figure we observe that the forward Euler method has a relative error four orders of magnitude greater than the 4^{th}-order Runge-Kutta method for each number of time steps. The error diminishes as we increase the number of time steps (i.e. decrease the stepsize). This is expected from the calculations of the global errors for the methods in section II. The discontinuity in the calculated data for the 4^{th}-order Runge-Kutta algorithm is due to the limited representation of floating point numbers in the memory of the computer. When the limited representations of the exact and numerical solutions are equal, the relative error will be exactly zero. This tells us that 4^{th}-order Runge-Kutta is a good approximation to the exact solution for our purposes.

We compare the trajectories computed by both methods in the z and x directions in Figure 3 and observe that the forward Euler method deviates noticeably in the x-direction, whereas the 4^{th}-order Runge-Kutta method does not. In the z direction it seems both methods are correctly approximating the analytical solution. However, looking at Figure 4 we see that forward Euler does in fact overshoot.

We noticed a discontinuity in the relative error of 4^{th}-order Runge-Kutta and attribute it to numerical errors. In calculating the relative error we subtract two quite identical numbers with each other, the analytical solution and the 4^{th}-order Runge-Kutta approximation. We can see from Figure 3 and Figure 4 that there is very little error on most part of the 4^{th}-order Runge-Kutta method. From these observations we see that

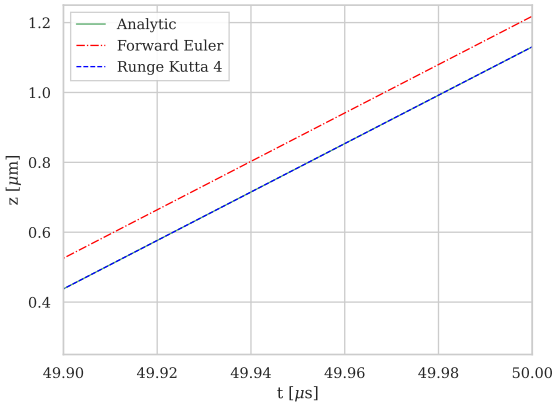

Figure 4: Zoomed in part of the last steps of the z direction in Figure 3a. We observe a deviation for the forward Euler method. We also notice that the 4^{th}-order Runge-Kutta method doesn't deviate here.

Table II: Convergence rate of the errors from the forward Euler (FE) and 4^{th}-order Runge-Kutta (RK4) methods.

Method	**Error convergence rate**
FE	1.46
RK4	1.27

compared to the 4^{th}-order Runge-Kutta method, forward Euler is a more error-prone method to choose for our purposes. We have also seen that the 4^{th}-order Runge-Kutta method is a great choice for this simulation judging by the relative error and computed trajectories.

From the different simulations at the different time steps seen in Figure 2 we found the rate of convergence of the error for each method. These can be found in table II. We observe that the error of the forward Euler method has a higher convergence rate than the error for 4^{th}-order Runge-Kutta method. This tells us that if we were to increase the number of step size for both methods then the forward Euler error would converge faster. However 4^{th}-order Runge-Kutta method still has a much smaller error for all the step sizes we have tested. The error convergence only tells us that if we increase the number of steps in the simulation, we expect the error of the forward Euler to get smaller faster than the error in 4^{th} Runge-Kutta.

The 3D trajectory of a single particle in Penning trap simulated with both methods can be seen in Figure 5, where we clearly see the difference between both methods for our simulations.

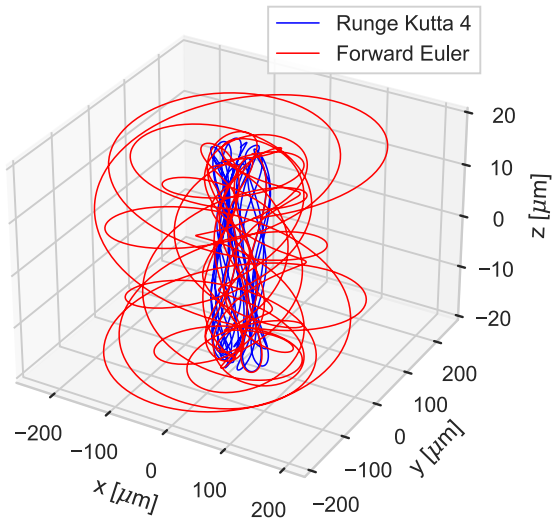

Figure 5: Trajectory of a single Ca+ ion in the Penning trap. We see the trajectory computed by the forward Euler and 4^{th}-order Runge-Kutta methods. The methods diverge greatly when taking into account all three directions of movement.

In Figure 6 we see the trajectories of two Ca^+ ions using 4^{th}-order Runge-Kutta. The initial position and velocity, charge and mass of these two particles can be found in table I. In this simulation we have excluded the Coulomb interactions between the ions. In Figure 6a we see that the particles both move in a very similar way. The similarity in their paths is expected, as they are both affected by the same electric and magnetic field, and not affected by each other. Their difference is due to their different initial conditions. The particles are affected by a force from the magnetic field, which is perpendicular to the xy-plane. This force will always be perpendicular to both the magnetic field $\vec{B}$ and the velocity $\vec{v}$ of the particle, and therefore acts as a centripetal force on the particles. This explains the particles' circular motion, which trace out a cyclotron motion in the xy-plane as expected[5].

We observe the oscillations the z direction in Figure 6b in addition to the cyclotron motion in the xy-plane. This is due to the electric potential in the Penning trap, which produces an electric force on each particle. If we look at the z-direction of this force (see equation (1)), it always points towards $z = 0$, which gives a harmonic oscillator where the particles oscillate in the z-direction with equilibrium at $z = 0$ in our case without friction forces.

In Figure 7a we see the trajectory of two particles, both simulated using 4^{th}-order Runge-Kutta method. In this simulation we have included the Coulomb force

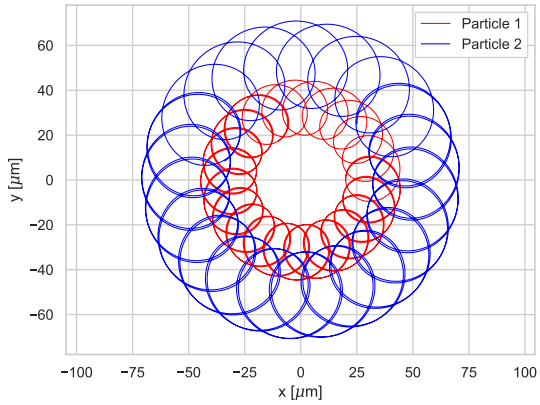

(a) Trajectories of both particles in the xy-plane.

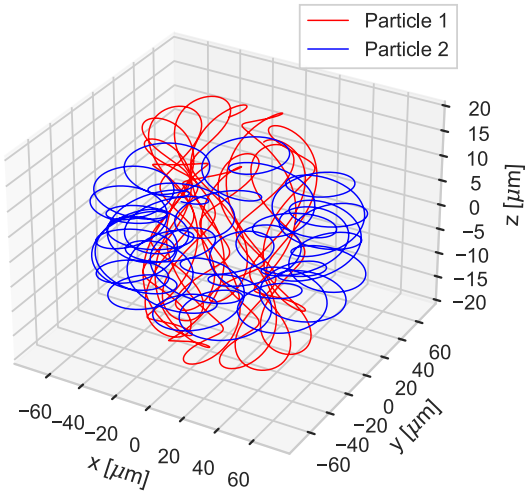

(b) Trajectories of both particles in three dimensions.

Figure 6: The trajectories of two particles in the Penning trap without Coulomb interactions between the particles. The trajectories are computed using 4^{th}-order Runge-Kutta. We have included the trajectories in both the xy-plane and in the three dimensional space. The initial position and velocity, charge and mass of these two particles can be found in table I.

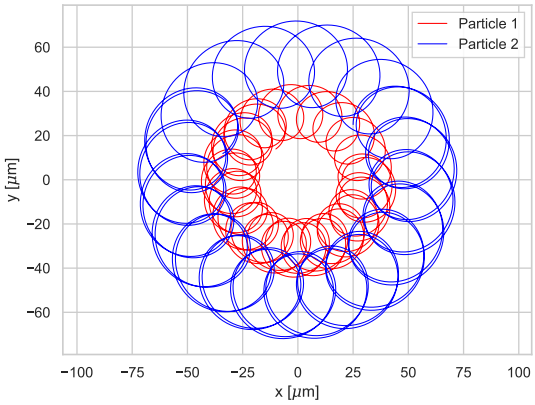

(a) Trajectories in the xy-plane of both particles with Coulomb interaction.

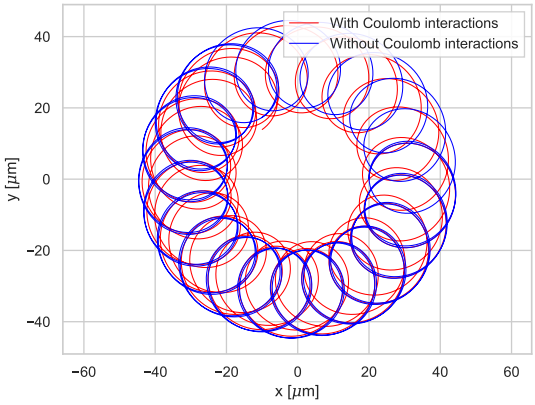

(b) Comparison between the trajectories of one ion when the ions are affected by the Coulomb interactions and when not. The red dot marks the initial position of the ion.

Figure 7: Comparison of the paths of two Ca+ ions simulated using 4^{th}-order Runge-Kutta method in the xy-plane. In this simulation we have included the Coulomb interactions between the two particles and used the same initial conditions as in Figure 7. In Figure 7a we see both particles' path. In Figure 7b we can compare the trajectory when affected by the Coulomb interactions and when not.

between the particles. If we compare the path the ions had without the Coulomb interactions, shown in Figure 7b, which has the same initial conditions, we see that they are quite similar. Their differences are expected as the ions now influence each other's paths. The difference is slight, though if we are to simulate with more ions, the Coulomb interactions between them will result in a more chaotic movement.

Looking at the phase space of both simulations of the two ions in the Penning trap, i.e. with and without the Coulomb interactions, in figures 8 and 9 we make similar observations. In the x direction, the phase space changes slightly, we cannot directly observe from these figures whether or not the energy is conserved. In the z direction however, the difference is noticeable. We see that the energy is conserved in the case where the ions do not interact with one another, the phase space of

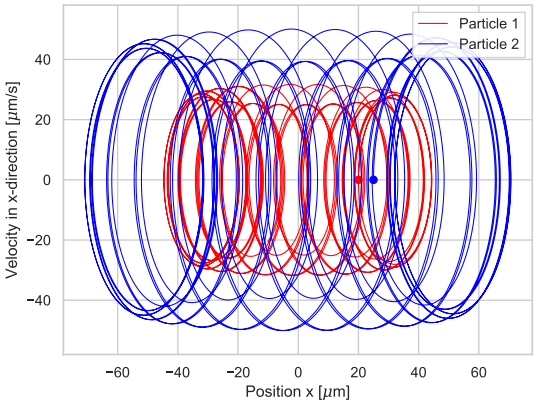

(a) Phase space in the x direction of both ions when they're not affected by the Coulomb interactions.

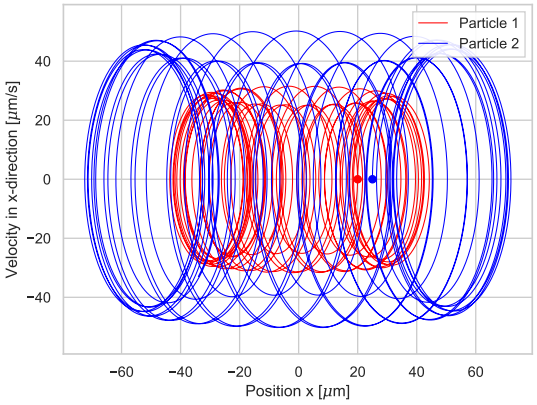

(b) Phase space in the x direction of both ions when they are affected by the Coulomb interactions.

Figure 8: Comparison of the phase spaces of two Ca+ ions simulated using 4^{th}-order Runge-Kutta method in the x direction. This the phase space for the same simulations used in Figure 7. The difference is slight between the two phase space's. The dots indicate the initial position of each particle, respective of colour.

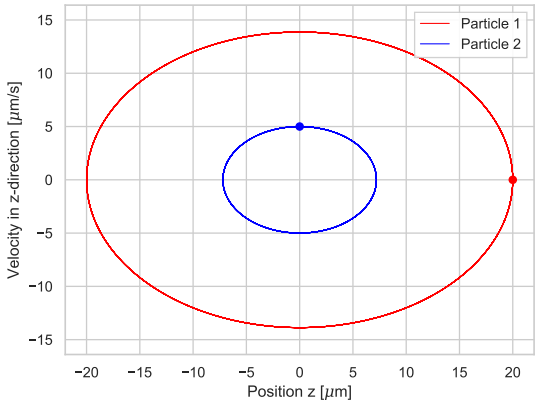

(a) Phase space in the z direction of both ions when they're not affected by the Coulomb interactions.

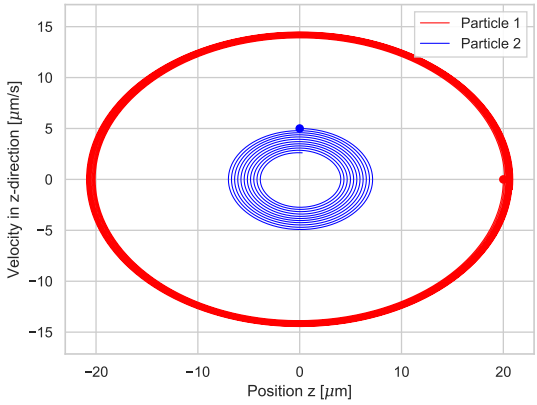

(b) Phase space in the z direction of both ions when they are affected by the Coulomb interactions.

Figure 9: Comparison of the phase spaces of two Ca+ ions simulated using 4^{th}-order Runge-Kutta method in the z direction. This the phase space for the same simulations used in Figure 7. The difference between the two simulations is noticeable. The dots indicate the initial position of each particle, respective of colour.

each particle shows a closed circle. When we include the Coulomb interactions we see that the phase space volume varies for both particles and so their individual energy in the z direction is not conserved. We notice that the phase space volume for particle 2 diminishes while that of particle 1 augments, this could indicate that the total energy in the z direction is conserved but the particles distribute it among themselves.

We simulated the system with a time-varying applied potential V_0, according to equation (6). The duration of the simulation was 500μs with a time step 0.02μs. We considered three different amplitudes $f \in 0.1, 0.4, 0.7,$ with angular frequencies $\omega_V \in [0.2, 2.5]$, and a step size $d\omega_V = 0.02$ MHz between each frequency. The simulation is only done for 25 particles as we felt like this number was the middle ground between good results and the cost in computation time. The fraction of particles still left inside the trap after 500μs is displayed in Figure 10. We see that by increasing the amplitude of the oscillation of the potential, the ranges where particles are pushed out gets wider.

From these simulations, we want to find the resonance frequencies that are particularly effective for pushing

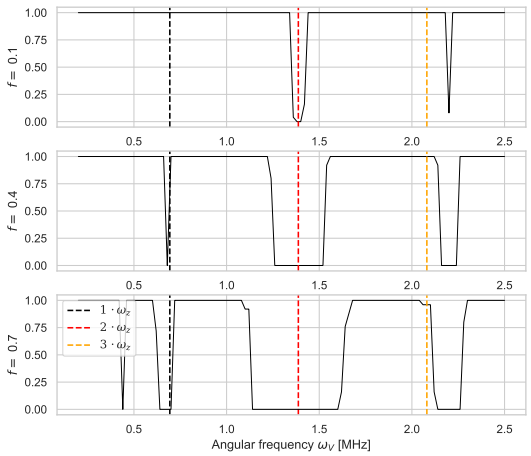

Figure 10: Graph of the fraction of particles that are still trapped after 500μs, for three different amplitudes $f \in 0.1, 0.4, 0.7$. The simulation contains 25 particles with a time step of $h = 0.01\mu$s. Step length between the angular frequencies is $d\omega_V = 0.02$ MHz.

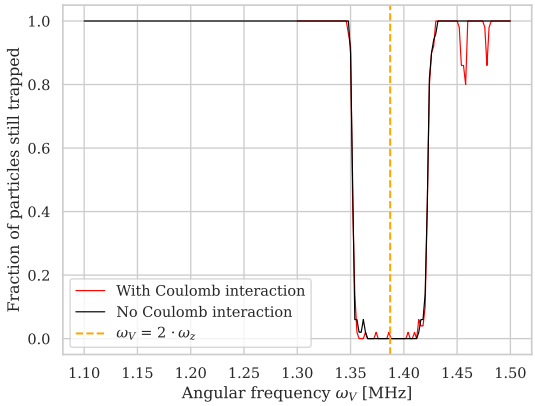

Figure 11: The fine scan of the frequencies for both interacting and non interacting particles. This is the fraction of the 50 initial particles that have escaped during the simulation for different frequencies of the varying electric field. The black line is for non interacting particles, the red for interaction and the orange dashed line is for where we expect the maximum resonance to kick out the most particles.

the particles out of the trap. In Figure 10, we see that for all three amplitudes f, all particles are pushed out of the trap at applied angular frequency $\omega_V \approx 1.6$ MHz. This can be interpreted as a resonance frequency for the driving applied force, amplifying the oscillatory motion until the particles is no longer contained within the characteristic dimension d of the trap.

From Figure 10, we see that in addition to $\omega_V \approx 1.6$ MHz, particles tend to escape at frequencies $\omega_V \approx 0.7$ and 2.3 MHz. In addition to the graph of particles, we show three multiples of the frequency ω_z as dashed vertical lines. We see that these multiples coincide well with the resonance frequencies. From the parameters of the system, we obtain a value of

$$\omega_z = \sqrt{\frac{2qV_0}{md^2}} \approx 0.6936 \frac{1}{\mu\text{s}} = 0.6936 \text{ MHz}$$

where $q = 1$ e, $V_0 = 2.41 \cdot 10^6 \ \frac{\text{u}(\mu\text{m})^2}{(\mu\text{s})^2\text{e}}$.

For a particle contained in the Penning trap with an oscillating applied potential, we can refer to the analytical solution as long as Coulomb interactions are neglected. From the constraint in equation 15, we see that as long as this inequality is fulfilled, the particle will be bound in the xy-plane.

However, this means that the resonance frequencies must amplify the oscillatory z-motion, so that the particles are pushed out along the z-direction.

We performed a fine-grained frequency scan around $\omega_V \in [1.3, 1.5]$ MHz, with step length $d\omega_V = 0.002$ MHz. For each frequency, we simulated 50 particles for a duration of 500μs with time step $dt = 0.01\mu$s. The fraction of particles left inside the Penning trap per frequency is shown in Figure 11. Once again, we see that as the angular frequency ω_V of the driving force approaches a multiple of the axial oscillating frequency ω_z, the particles are pushed outside the Penning trap. The fraction of particles still left when Coulomb interaction is taken into consideration, is shown as the red line in Figure 11. Due to this interaction, there are still some particles left inside the trap as $\omega_V \to 2\omega_z$. In addition, we see that towards the end of the frequency range, some particles are thrown out even though the applied oscillation ω_V does not coincide with the resonance frequency of the axial oscillatory motion. This may be caused by the interacting particles pushing each other out due to particle-particle-repulsion.

IV. CONCLUSION

What we have found is a description of a charged particle in a Penning trap. The path of the particle, we have shown, can be quite complex. However, by simplifying to the case of s single particle in the xy-plane, we can solve the equations of motion analytically. In addition, we have solved the motion numerically using the forward Euler and the 4^{th} order Runge-Kutta algorithms. Through our simulations we have found that the 4^{th} order Runge-Kutta method far exceeds the accuracy of the forward Euler method. We also found that

the the 4^{th} order Runge-Kutta method fits quite well to the analytical description of the particle movement. The error convergence rates for forward Euler and the 4^{th} order Runge-Kutta are 1.46 and 1.27 respectively.

Further, we have found that by subjecting the simulated particles to an oscillating applied potential, there exists oscillating frequencies that are particularly well-suited for pushing the particles outside of the trap. These frequencies are the multiples of the angular axial frequency of the particles $\omega_V \approx 0.6936$ MHz. These applied potentials cause resonance in the axial motion of the particle, pushing them out in the z-direction. For particles that interact through the Coulomb force, we find that not all particles are guaranteed to be pushed out at the resonance frequencies. Instead, we find that the Coulomb interaction causes the motion of the particles to behave less predictably.

---

[1] F. Penning, Physica **3**, 873 (1936).

[2] NobelPrize.org., "`https://www.nobelprize.org/prizes/physics/1989/summary/`," (2022), last accessed 25 October 2022.

[3] G. Schneider *et al.*, Science **358**, 1081 (2017), https://www.science.org/doi/pdf/10.1126/science.aan0207.

[4] A. K. Akriesch, "`https://commons.wikimedia.org/wiki/File:Penning_Trap.svg`," (2008), last accessed 13 October 2022.

[5] L. S. Brown and G. Gabrielse, Rev. Mod. Phys. **58**, 233 (1986).

Appendix A

We derive the differential equations governing the time evolution of the position of a particle in the Penning trap. The particle is subject to a Lorentz force due to the applied electric and magnetic fields. Newton's second equation yields that the sum of the forces for a particle equals

$$\begin{aligned} m\ddot{\boldsymbol{r}} &= \boldsymbol{F} = q\boldsymbol{E} + q\boldsymbol{v} \times \boldsymbol{B} \\ &= q\boldsymbol{E} + q\boldsymbol{v} \times \boldsymbol{B} \end{aligned} \tag{A1}$$

First we write out the electric field vector $\boldsymbol{E}$:

$$\begin{aligned} \boldsymbol{E} &= -\nabla V \\ &= -\Big(-\frac{2V_0}{2d^2} x\ \boldsymbol{e}_x - \frac{2V_0}{2d^2} y\ \boldsymbol{e}_y + \frac{4V_0}{2d^2} z\ \boldsymbol{e}_z \Big) \\ &= \frac{V_0}{d^2} x\boldsymbol{e}_x + \frac{V_0}{d^2} y\boldsymbol{e}_y - \frac{2V_0}{d^2} z\boldsymbol{e}_z \\ &= \frac{V_0}{d^2}\big(x\boldsymbol{e}_x + y\boldsymbol{e}_y - 2z\boldsymbol{e}_z\big) \end{aligned} \tag{A2}$$

In order to compute the Lorentz force, we also write out the cross product $q\boldsymbol{v} \times \boldsymbol{B}$, where $\boldsymbol{B} = B_0\boldsymbol{e}_z$, which yields

$$\begin{aligned} q\boldsymbol{v} \times \boldsymbol{B} &= q\big(\dot{y}B_0\ \boldsymbol{e}_x + \dot{x}B_0\ \boldsymbol{e}_y\big) \\ &= qB_0\big(\dot{y}\ \boldsymbol{e}_x + \dot{x}\ \boldsymbol{e}_y\big) \end{aligned} \tag{A3}$$

Considering only the x-component of Newton's second law in equation (A1), we derive an expression for the acceleration of the particle:

$$\begin{aligned} m\ddot{x} &= q\frac{V0}{d^2}x + \dot{y}qB0 \\ \ddot{x} &= q\frac{V0}{md^2}x + \dot{y}qB0\frac{1}{m} \\ &= \frac{1}{2}\omega_z^2 + \omega_0\dot{y} \\ \Rightarrow\ \ddot{x} - \omega_0\dot{y} - \frac{1}{2}\omega_z^2 x &= 0 \end{aligned} \tag{A4}$$

where we have defined $\omega_0 = \frac{qB_0}{m}$ and $\omega_z^2 = \frac{2qV_0}{md^2}$ in order to simplify the expression. Similarly, the equation of motion for the y-component becomes

$$\begin{aligned} m\ddot{y} &= q\frac{V0}{d^2}y - \dot{x}qB0 \\ &= \frac{1}{2}\omega_z^2 y - \omega_0\dot{x} \\ \Rightarrow\ \ddot{x} + \omega_0\dot{x} - \frac{1}{2}\omega_z^2 y &= 0 \end{aligned} \tag{A5}$$

and lastly, for the z-component we get

$$\begin{aligned} m\ddot{z} &= q\frac{2V_0}{d^2}z \\ \Rightarrow\quad \ddot{z} &= \omega_z^2 z \end{aligned} \tag{A6}$$

We see that equation (A4) and equation (A5) are coupled, meaning dependent of each other. These two equations can be combined by extending the mathematics into the complex plane, such that $f(t) = x(t) + iy(t)$ is a complex

function with the x-position as its real part and y-position as its imaginary part. Differentiating $f(t)$ twice with respect to time gives

$$\begin{aligned}\ddot{f} &= \frac{d}{dt}\Big(\dot{x} + i\dot{y}\Big) \\ &= \ddot{x} + i\ddot{y} \\ &= \omega_0\dot{y} + \frac{1}{2}\omega_z^2 x + i\Big(- \omega_0\dot{x} + \frac{1}{2}\omega_z^2 y\Big) \\ &= \omega_0(\dot{y} - i\dot{x}) + \frac{1}{2}\omega_z^2(x + iy)\end{aligned} \tag{A7}$$

Using $i\dot{f} = i\dot{x} - \dot{y}$, we obtain a single complex differential equation

$$\begin{aligned}\ddot{f} &= -i\omega_0\dot{f} + \frac{1}{2}\omega_z^2(x + iy) \\ \Rightarrow\ \ddot{f} &+ i\omega_0\dot{f} - \frac{1}{2}\omega_z^2 f = 0\end{aligned} \tag{A8}$$

The general analytical solution to this differential equation is given by

$$f(t) = A_+ e^{-i(\omega_+ t + \phi_+)} + A_- e^{-i(\omega_- t + \phi_-)} \tag{A9}$$

where ϕ_+, ϕ_- are constant phases and A_+, A_- are positive amplitudes that characterizes a specific solution.

In order to obtain a bounded solution for the motion in the xy-plane, we require that $|f(t)| < \infty$ as $t \to \infty$. From , we see that the absolute value of $f(t)$ diverges if $\omega_\pm$ is a multiple of i. Therefore, we must ensure that $\omega_\pm$ is real for any ω_0, ω_z. This constraint means that

$$\begin{aligned} Im\big[\omega_\pm\big] &= Im\left[\frac{\omega_0 \pm \sqrt{\omega_0^2 - 2\omega_z^2}}{2}\right] = 0 \\ \Rightarrow\ \ \omega_0^2 - 2\omega_z^2 &> 0 \\ \Rightarrow\ \ \omega_0^2 &> 2\omega_z^2\end{aligned} \tag{A10}$$

since we know that $\omega_0 = \frac{qB_0}{m}$ is a real number.

This allows us to relate the Penning trap parameters (B_0, V_0, d) to the properties of the particle (q, m) such that

$$\begin{aligned}\omega_0^2 = \Big[\frac{qB_0}{m}\Big]^2 &> \frac{4qV_0}{md^2} = 2\omega_z^2 \\ \frac{qB_0}{m} &> \frac{4V_0}{d^2} \\ \frac{q}{m} &> \frac{4V_0}{B_0 d^2}\end{aligned} \tag{A11}$$

As long as the preceding inequality is fulfilled, motion of the particle will be bound in the xy-plane.

Further, we want to find the upper and lower bounds on the distance between the particle and the origin in the xy-plane. Let R_+ and R_- be the upper and lower bounds respectively. The absolute value $|f(t)|$ can then be written as

$$\begin{aligned}|f(t)| &= \sqrt{f(t)^* f(t)} \\ &= \sqrt{A_+^2 + A_-^2 + 2A_+A_- \cos\Big[- (\omega_+ t + \phi_+) + (\omega_- t + \phi_-)\Big]}\end{aligned} \tag{A12}$$

Since we know that the domain of the cos-function is $[-1, 1]$, we get that $|f(t)|$ attains its maximum when $\cos\Big(\omega_+ t + \phi_+\Big)$ equals 1, which will be when $\omega_+ t + \phi_+$ equals $2\pi m$, for an even integer m. In that case, we get

that the maximum is

$$\begin{aligned} |f(t)|_{max} &= \sqrt{A_+^2 + A_-^2 + 2A_+A_-} \\ &= \sqrt{(A_+ + A_-)^2} \\ \Rightarrow |f(t)|_{max} &= A_+ + A_- \end{aligned} \tag{A13}$$

Further, the lower bound of $|f(t)|$ will be when the cos-expression equals -1. In that case,

$$\begin{aligned} |f(t)|_{min} &= \sqrt{A_+^2 + A_-^2 - 2A_+A_-} \\ &= \sqrt{(A_+ - A_-)^2} \\ \Rightarrow |f(t)|_{min} &= |A_+ - A_-| \end{aligned} \tag{A14}$$